Quantum jumps and the single trapped barium ion: Determination of collisional quenching rates for the $5d\ ^2D_{5/2}$ level

A. A. Madej and J. D. Sankey
Time and Length Standards, Laboratory for Basic Standards, National Research Council of Canada, Ottawa, Canada K1A 0R6
(Received 12 September 1989)

A single Ba^+ atom was confined in a radio-frequency ion trap and cooled by near-resonant laser light. Quantum jumps into and out of the metastable $5d\ ^2D_{5/2}$ level were observed that followed the expected exponential distribution in dark periods to good agreement. Measurement of quantum-jump distributions together with careful measurements of the absolute partial pressures of all residual gas species enabled accurate measurements of the quenched $5d\ ^2D_{5/2}$ lifetime as a function of quenching gas pressure. Measurements of quenching were observed at pressures where the mean collision rate was on the order of 1 s^{-1}. The results yielded quenching rate constants for the metastable level for a series of gases that typically make up the residual gas environment of ultra-high-vacuum systems (H_2, He, CH_4, H_2O, CO, N_2, Ar, and CO_2) together with an improved value of the $5d\ ^2D_{5/2}$ radiative lifetime of $t_0=34.5\pm3.5$ s. The above quenching rate constants were then compared with classical ion-molecule collision theory. It was found that the quenching rates for molecular gases were comparable to the classical collision rates, while the rates for atomic gases were considerably lower.

I. INTRODUCTION

The realization of the confinement and observation of single ions has provided new opportunities in laser spectroscopy and studies of atomic physics at the single-atom level.[1,2] Long interrogation and confinement times for the ion allow the possibility to examine transitions with very narrow linewidths without transit-time broadening.[3] The use of laser cooling has enabled reductions in the ion kinetic energy into the millikelvin level thus avoiding problems encountered with Doppler broadening and shifts. Some transitions for trapped ions have been suggested as frequency standards.[3-5] In addition, studies of single ions have enabled the observation of "quantum jumps" into and out of the ion's metastable state by monitoring the interruption of fluorescence from the ion cycling on a strongly allowed transition.[6-8] Not only has this effect been a source of theoretical discussion,[9-11] it allows the unique possibility of monitoring the ion's internal state. It is possible to observe whether the ion has undergone an excitation into the metastable level via a weak transition with near unity detection efficiency.[3] By being able to monitor the single ion's internal state under such well-controlled conditions, one is also able to study the effects of the ion's external environment upon the atomic system. Previous observations of quantum jumps from the Ba^+ atom by Nagourney, Sandberg, and Dehmelt[6] and Sauter *et al.*[12] have shown a sensitivity to quenching collisions affecting the long $5d\ ^2D_{5/2}$ metastable lifetime ($t=35$ s). In our present work, we have examined the effect of background gas collisions on the ion by observing the quantum jump statistics of the barium ion subject to the presence of buffer gases at pressures (10^{-8}–10^{-5} Pa) where the mean binary collision time is on the order of the $5d\ ^2D_{5/2}$ radiative lifetime. From this work, we have obtained a value for the natural radiative lifetime of the $5d\ ^2D_{5/2}$ level and accurate quenching rates of the metastable level for gases which typically make up the residual gas environment of high vacuum systems (H_2, N_2, CO, CO_2, CH_4, He, Ar, and H_2O). The determined quenching rate constants were then compared with classical ion-molecule collision theory. The results show that the quenching rates for molecular background gases are comparable to the classical ion-molecular rates, while the observed rates for atomic gases such as He and Ar are two orders of magnitude below the classical collision rates.

II. EXPERIMENTAL PROCEDURE

A. Experimental apparatus

The confinement of the single Ba^+ atom is provided by a small radio-frequency (rf) trap. The construction of the trap is similar to that used by others[6,13,14] in single-ion-trapping and laser-cooling experiments and is shown in cross section in Fig. 1. The ring and endcap electrodes are formed from nonmagnetic stainless steel with the endcap electrodes (type 303 stainless) possessing a hemispherical surface of $r=1.4$ mm radius of curvature, while the ring electrode was formed from a 2-mm-thick plate (type 304 stainless), which had a 1.4-mm hole drilled and later machined into semicylindrical cross section. The characteristic trap dimensions from trap center to the endcap and ring electrodes were $z_0=1.0$ mm and $r_0=1.4$ mm, respectively. An applied rf drive voltage of $V_0=300$ V amplitude at a frequency of $f_0=5.0$ MHz was employed. Under such conditions, the effective pseudopotential well depth[15] in the axial and radial directions is calculated to be $D_z=15.9$ V and $D_r=8.0$ V. A nearby

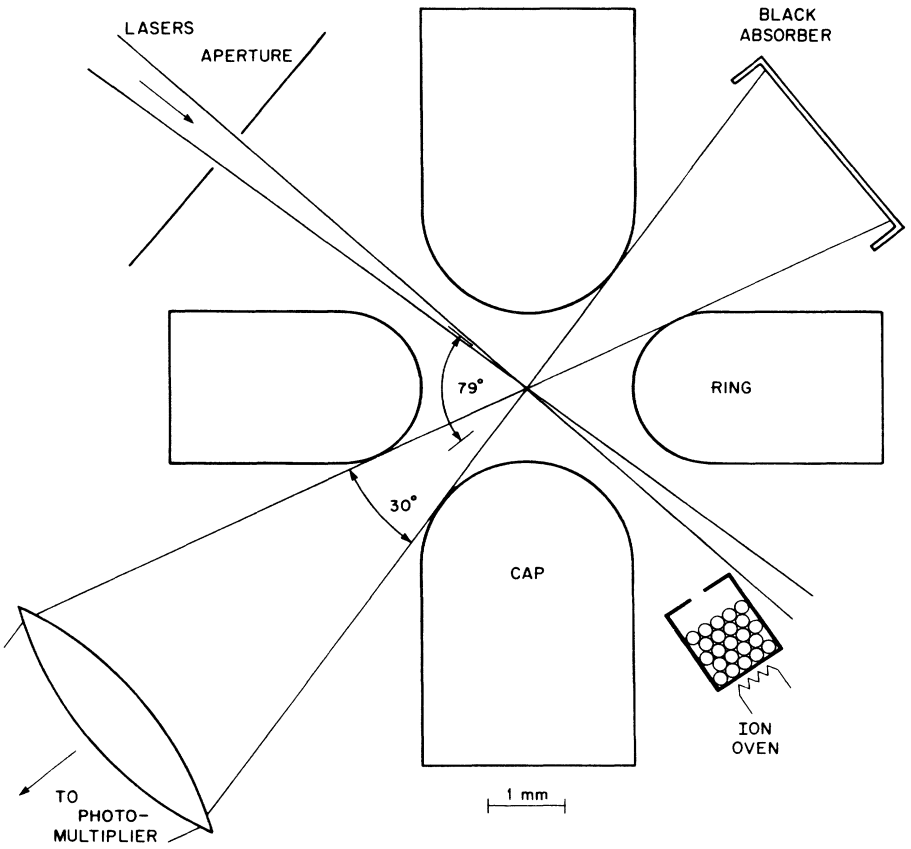

FIG. 1. Cross-sectional view of ion trap electrodes together with laser excitation beam and ion fluorescence collection angles.

oven biased negative ($V=-60$ V) relative to the ring-electrode potential produced beams of both neutral barium and electrons which provided a simple technique for the formation of single ions in the trap under high vacuum conditions ($P<10^{-7}$ Pa).[16] Laser cooling and fluorescence excitation of the barium ion was provided by excitation on the $6p\,^2P_{1/2}-6s\,^2S_{1/2}$ ($\lambda=493.5$ nm) and the $6p\,^2P_{1/2}-5d\,^2D_{3/2}$ ($\lambda=650.0$ nm) transitions (see Fig. 2) from two commercial ring dye lasers (Coherent 699-21). The 493.5-nm radiation was provided by pumping a Coumarin 102 dye solution using multiline violet radiation at 3.0 W from a commercial Kr^+ laser thus providing 100 mW output power. The desired 650-nm light was provided by pumping a dye solution of DCM with 5.0 W at 514 nm from a commercial Ar^+ laser, giving a dye laser output power of 300 mW. With the use of these pump sources and laser dyes, operating periods of up to 50 h could be achieved without dye change and observed ion storage times up to 12 h were obtained. Characteristic linewidths from the dye lasers were on the order of 1 MHz. The output from the two dye lasers were attenuated and collinearly overlapped before being focused within the trap vacuum chamber. During the present experimental work, an excitation beam of diameter of $D=250$ μm was used to illuminate the trap center with incident laser powers being 10–100 μW. The detection of the ex-

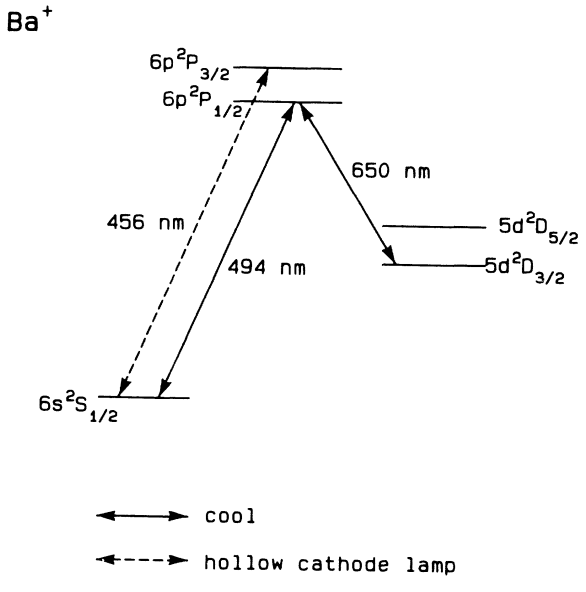

FIG. 2. Partial energy-level diagram of Ba^+ showing laser excitation and cooling transitions together with the lamp excited transition used for excitation into the $5d\,^2D_{5/2}$ level.

cited Ba^+ atom was achieved by blocking all but the desired 493-nm S-P fluorescence with a narrow band filter and by imaging the trap center on a pinhole aperture, which was located in front of a photon counting photomultiplier (Hamamatsu R646) system (see Fig. 3). The output from the photomultiplier was fed into a matched preamplifier (Hamamatsu C716) and the resulting signal was sent into a single channel analyzer (Canberra 2015A). Detected counts were then converted into an analog count rate signal via a ratemeter (Canberra 1481L). The effective ratemeter time constant was $t_c = 0.4$ s. The output photon counting rate from the ion could then be stored by computer or displayed on a chart recorder. The total efficiency of the system including light collection solid angle, filter losses, and photomultiplier sensitivity is estimated to be 2×10^{-3}.

For efficient laser cooling,[17] both lasers tuned to the S-P and P-D transition were detuned slightly below line center by approximately -20 MHz. Due care was exercised to avoid the condition of equal detuning of the S-P and P-D transitions where coherence effects between the two driving fields interacting with the atom produce a null in the P state population and reduce the detected S-P photon rate.[14,18] Examinations of the P-D line shape were performed by fixing the frequency of the 494-nm source near line center and scanning the 650-nm laser frequency through the resonance. It was observed that the line shape envelope followed a smooth Voigt-type profile for frequencies up to the resonance line center. The fluorescence rapidly dropped for detunings above line center corresponding to laser heating of the ion. No evidence of micromotion broadening or line splitting of the line shape[14] (due to the ion being displaced from the center of the rf quadrupole field) was observed, and possible resulting Stark effects on the metastable D level are considered negligible. From the line-shape measurements, an upper limit to the kinetic temperature of $T < 10$ K has been determined. As a final note, a weak magnetic field of 5×10^{-5} T was present along the incident laser direction. This field is employed to prevent optical pumping of the Ba^+ into the $m_J = \pm\frac{3}{2}$ sublevels of the $^2D_{3/2}$ state.[14]

Excitation into the $5d\,^2D_{5/2}$ metastable level was provided by weak excitation of the $6s\,^2S_{1/2}$–$6p\,^2P_{3/2}$ ($\lambda = 456$ nm) level, which can relax into the $5d\,^2D_{5/2}$ level by radiative decay. A commercial barium hollow cathode lamp was used to provide the desired excitation at 456 nm. The light from the lamp was filtered and weakly focused into the ion trap chamber. The lamp provided excitation into the metastable level at a rate of 0.1 s^{-1}. Mechanisms of excitation into and out of the level by Raman-Stokes transitions of the driving laser fields (see the Appendix) were of negligible effect.

B. Measurement of gas partial pressures and calibration of gauges

One of the most critical parameters required in the present study was the accurate measurement of the absolute partial pressures of the gas species present during a particular quenching study. In our vacuum system, the ion trap was housed in a chamber formed from a stainless steel block which has three orthogonal channels of $r = 1.7$ cm bored, thus allowing six access ports into the chamber. Two ports possessed Brewster windows for the input and exit of the excitation and cooling radiation, while a third window was used as the port for fluorescence detection. At the rear of the trap chamber, a multicross port of $r = 1.7$ cm was connected. This port led individually to the vacuum gauges and analyzer, the titanium sputter-ion triode pump (Varian No. 911-5030, rated at 15 l/s for N_2), and a low-flow-rate leak valve (Varian No. 951-5106). The individual lengths of the tubing from the center of the multicross port were 10 cm to

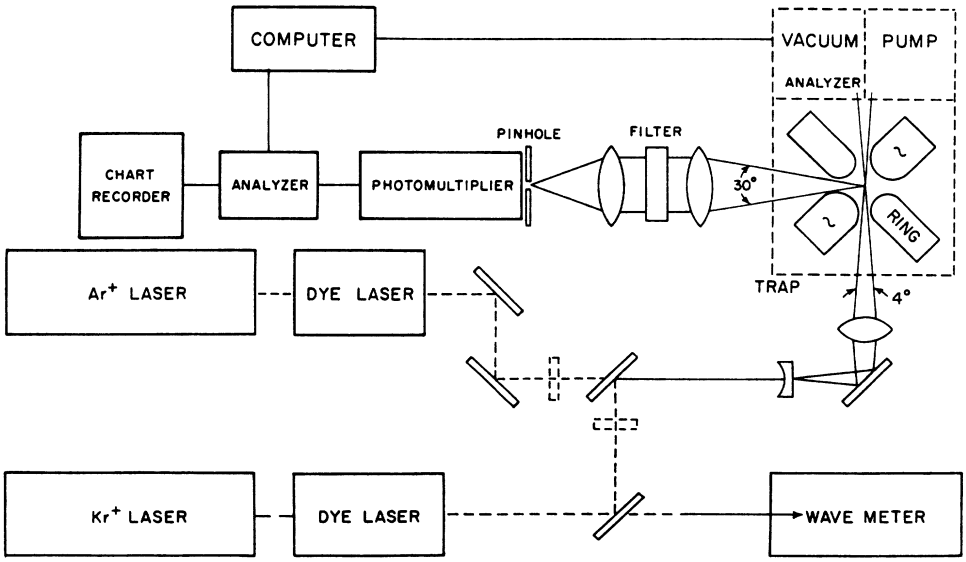

FIG. 3. Schematic diagram of experimental setup.

the trap chamber, 13 cm to the gauges, and 32 cm to the ion pump. During experimental runs the total pressure and gas composition were monitored by an ion gauge and mass spectrometer. The ion gauge used was a nude Bayard-Alpert type (Granville-Phillips No. 274 023), which we fitted with a thoria coated tungsten filament designed for low operating temperatures, while the gas analyzer (Anatek Dycor M100) was a quadrupole mass spectrometer. The gas leak valve opened directly into the multicross port, thus the only pressure difference from pumping the inlet gas was due to the pumping of the gauges across the impedance of the 13-cm tube and of outgassing of the trap chamber across the impendance of the 10-cm tube. Measuring these effects and taking the system conductances into account yielded the result that these effects were negligible ($<1\%$ of gauge readings) in comparison to the relative and absolute errors of the gauges.

During experimental runs, a particular gas was employed from the ones used in our study (H_2, He, CO, CH_4, N_2, H_2O, Ar, and CO_2, $>99\%$ purity) and introduced through the leak valve. At each setting of the valve, the ion gauge was read and an analyzer scan was taken of the individual masses of interest. The lowest pressures attained in our study were in the vicinity of 3×10^{-8} Pa. In most gas studies, pressures in the region of 10^{-7}–10^{-6} Pa were used. For He and Ar, the quenching rates were found to be quite low (10^3 s^{-1} Pa^{-1}), thus pressures in the range of 10^{-6}–10^{-5} Pa were employed. In order to obtain reliable absolute pressure readings for our residual gases in the experimental chamber, a calibration of our system was performed in conjunction with our Laboratory for Basic Standards pressure group. A detailed description of the calibration procedure has been given elsewhere.[19] Briefly, initial linearity and calibration of our ion gauge were measured over the range of 10^{-6}–10^{-3} Pa in N_2 using a Knudsen expansion apparatus. Linearity of the mass spectrometer was performed by calibrations of the mass spectrometer versus ion gauge for the gases used. Absolute calibration of the individual gas pressures were obtained using a spinning rotor gauge transfer standard. The spinning rotor gauge was calibrated relative to the Knudsen expansion apparatus over the range of 10^{-4}–100 Pa. An intercomparison of the ion gauge and the rotor gauge was performed in our experimental chamber using all gases employed in the present quenching measurements by taking comparison readings of three per decade from 6×10^{-4} to 10^{-1} Pa. The ion gauge was then used to transfer the rotor gauge calibrations down into the ultra-high-vacuum region (10^{-7}–10^{-5} Pa). In summary, the best one-σ reproducibility of the mass spectrometer was $\pm10\%$ over 0.1–20 μPa. The accuracy of the calibration overall is $\pm13\%$ of total pressure.

C. Experimental procedure and correction of observed dark periods

In the present experimental study, the quenching rate coefficients for the $^2D_{5/2}$ level of Ba^+ were determined by measuring the lifetime of the metastable level as a function of the partial pressure of a particular quenching gas. Due to the presence of a number of residual gases at high vacuum, partial pressures of all mass species were measured during each experimental run. Quantum jump data sets recording the duration of each dark period of approximately 50 jumps were taken at each applied pressure. It was possible to control the excitation rate into the $5d\,^2D_{5/2}$ level by adjusting the intensity of the resonant $^2S_{1/2}$–$^2P_{3/2}$ light being emitted by the hollow cathode lamp. Typical excitation into the $^2D_{5/2}$ level during these studies were 0.05–0.1 s^{-1}. With any one particular gas study, at least ten data sets were collected. Measurement of the dark period duration was performed by a computer monitoring the fluorescence signal provided by the count rate meter. Due to the time constant of the counting system, a transition from the fluorescing state at count rate r_i+r_d to the dark state r_d (r_d is due to the background scattered light into the detector) is considered to occur when the observed count rate is less than $r_i/e+r_d$. Return to the fluorescing state is defined as the time the count rate returns to $r_i(1-1/e)+r_d$. For an ideal system with a time constant t_c, the observed time T_0 corresponding to an actual dark period duration T would be

$$T_0=t_c\ln[\exp(T/t_c)-1]\ . \tag{1}$$

For our system, the time clock is updated only at 0.1-s intervals. The count rate meter has filter circuits as well as a count integration time constant. Due to these factors, observed dark times shorter than $T_0<0.5$ s were not recorded by the system. It can be shown[20] that for an exponential distribution $W_{\rm off}=R_-\exp(-R_-T)$ the mean of values T larger than t_c is

$$\mu_L=1/R_-+t_c\ . \tag{2}$$

(The modified distribution remains exponential in form and the mean is simply shifted by the new origin t_c.) We may thus correct for our measured mean by simply subtracting our chosen lower limit period t_c. Although formula (1) may be used in correcting the measured dark times for our quantum jump data, a further calibration was performed of the count-rate meter using a 1-kHz pulse train (simulating the 1500 cps of the ion fluorescence), which was interrupted for known periods T. A calibration curve of the observed versus applied dark times was obtained and used to obtain actual dark times from the observed values. A similar calibration was performed for short bright times. From this calibration, the estimated error in calculating T from T_0 is 0.05 s for $T_0>0.5$ s. Finally, if the strong fluorescence bright times between two successive quantum jumps were to be so short that it was not registered, the result would yield a dark time of improper long duration. It can be shown that the probability of an undetected double jump[9] into the $^2D_{5/2}$ level is

$$P_2(t_d)=\frac{R_+R_-\{[t_d(R_+-R_-)-1]\exp(-R_-t_d)+\exp(-R_+t_d)\}}{(R_+-R_-)^2}\ , \tag{3}$$

where R_+ and R_- are the excitation rate into and out of the metastable level and t_d is the minimum high fluorescence period detectable. In our case $t_d=0.6$ s and for the values of R_+ and R_- used in our experiment, the corrections arising from this effect are less than 2%, much smaller than the statistical uncertainty of the lifetime due to the finite data set.

For the studies with CO_2, a number of anomalous dark periods were observed. This effect has been explored in detail[20] and has been ascribed to the Ba^+ being "shelved" into a long-lived metastable complex which is then destroyed by a subsequent collision and returns to fluorescence (see Sec. III D). To remove these anomalous dark times from our data, we note that the mean of an exponential distribution $W_{\rm off}=R_-\exp(-R_-T)$ truncated above $T=u/R_-$ is

$$\mu_u=(1/R_-)\frac{1-\exp(-u)(1+u)}{1-\exp(-u)}\ . \tag{4}$$

Dark periods much larger than $1/R_-$ may be separated from the $^2D_{5/2}$ dark periods by an appropriate choice of u. A χ^2 test was used for this purpose.[20] The most probable lifetime of the metastable state may be calculated from the jumps by setting $u=4.5$ and employing values below $T=u/R_-$.

III. RESULTS

A. Observation of quantum jumps

An example of the observed quantum jumps in fluorescence signal of the ion excited into the $5d\ ^2D_{5/2}$ level is shown in Fig. 4. As can be seen, the ratio of the detected ion signal (r_i) of 1100 s^{-1} to the background scattered signal (r_d) (about 400 s^{-1}) is very good, enabling unambiguous identification of the fluorescing and dark periods for the ion. Figure 4(a) shows a portion of the observed jumps in fluorescence at the lowest pressures used in our study (30 nPa). The quantum jump durations are typically on the order of tens of seconds for these pressures and the average dark period for this data run was $t=32$ s, very close to the determined natural radiative lifetime of the $5d\ ^2D_{5/2}$ level (34±3 s). Figure 4(b) illustrates the effect of quenching gases added to the chamber. The total pressure during trace (b) was 4×10^{-6} Pa with the principal gas constituents being N_2 and H_2. A dramatic reduction in the mean dark period is observed due to collisional quenching reducing the lifetime to $t=5$ s. The incomplete descent of fluorescence levels in the short quantum jumps are due to time constant effects of the counting system. For our quenching measurements, pressures were selected such that the mean dark period was much longer than the time constant of the system and time constant effects were corrected and accounted for using the method outlined in Sec. II C.

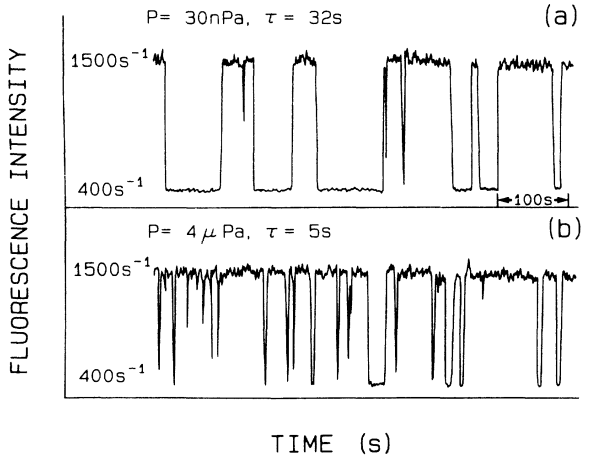

FIG. 4. Observed quantum-jump dark periods in the $6p\ ^2P_{1/2}-6s\ ^2S_{1/2}$ fluorescence due to excitation into and out of the $5d\ ^2D_{5/2}$ metastable level at background pressures of (a) 30 nPa and (b) 4 μ Pa. The time constant of the fluorescence detection system is 0.4 s.

B. Quantum jump distributions

The theoretical discussion of the observation of quantum jumps and their anticipated distribution of dark times have been the subject of a number of analyses.[9–11] For our case of weak, broad bandwidth excitation into the metastable level,[10] the distribution of observed "dark periods" in the strong fluorescence is given by

$$W_{\rm off}=R_-\exp(-R_-T)\ , \tag{5}$$

where T is the dark period duration and R_- is the rate of decay out of the metastable state. This decay rate is the sum of the natural radiative lifetime ($1/t_0$) and the effect of the individual quenching gases

$$R_-=(1/t_0)+\sum_i R_{Q,i}P_i\ , \tag{6}$$

where $R_{Q,i}$ is the quenching coefficient and P_i is the partial pressure of the individual gas. For an exponential distribution such as in (5), the mean value is equal to $1/R_-$ and possesses a statistical variance of R_-^{-2}. An example of the observed distributions is shown in Fig. 5. The figure shows the observed dark period distribution obtained from our data in the lowest pressures utilized in our study (4×10^{-8} Pa). χ^2 tests of the data for these and other quantum jump data sets gave probabilitimes of following an exponential dependence in excess of 0.95. As an illustration of the linearity of the quenching rate, Fig. 6 shows the determined rate of decay from the $5d\ ^2D_{5/2}$ level as a function of partial pressure where H_2 was used. The dashed line shown is the fitted curve using final values of our quenching rate coefficient for H_2. Due to the presence of a number of other residual quenching

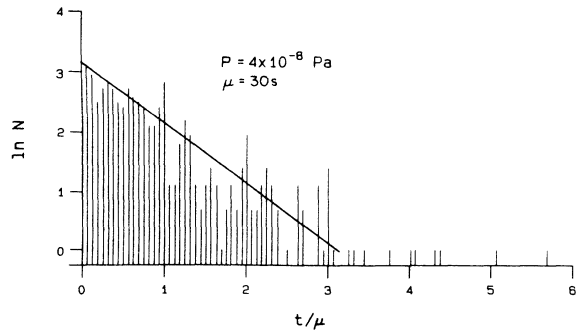

FIG. 5. Distribution of dark periods for a single Ba^+ atom at low pressure showing single exponential character (mean $=\mu=30$ s).

gases at high vacuum, gas pressures of all mass species were measured during an experimental run and a full multivariate linear regression fit was performed on our quantum jump data (about 10^4 jumps comprising studies with eight different gases). In the multivariative fit, the quenching coefficients of H_2, He, CH_4, CO, and N_2 were employed as free variables. Due to the presence of anomalous dark periods in the CO_2 data (see Sec. III E), the CO_2 quenching coefficient was determined separately and the correction for CO_2 partial pressure was applied to the multivariate fit. The H_2O partial pressure was kept sufficiently low so that its effect could be ignored except when it was the gas being studied. Also, an estimate of the quenching rate coefficient of Ar for the $5d\ ^2D_{5/2}$ level was made based on the determined quenching rates for the other gases.

C. Quenching coefficients of the $5d\ ^2D_{5/2}$ and the natural radiative lifetime

The results of the multivariate fit for the quenching coefficients are given in Table I and plotted in Fig. 7. The temperature of the background quenching gases in this study were $T=298\pm3$ K. Also given in Table I are the determined quenching rate constant and the cross section for quenching. The uncertainties for the rate constants for most gases were dominated by the uncertainty in the absolute pressure calibration (13%). For the case of CO_2 there existed slightly higher uncertainties in the absolute pressure calibration[19] resulting in total uncertainties of 18%, while for He the statistical uncertainties in the fitting resulted in a higher ascribed uncertainty of 25%. From the results, the largest quenching rates are observed for CH_4 and H_2O at $1.5\times10^5\ s^{-1}\ Pa^{-1}$. H_2 also possesses a large quenching rate coefficient due to its low mass and CO_2, CO, and N_2 appear to have comparable rates. As expected, the quenching rate coefficient for He is very small [$2400\pm(25\%)\ s^{-1}\ Pa^{-1}$]. Also from the multivariate fit, it was possible to extract the natural radiative lifetime of the metastable level at zero total pressure. A value of $t_0=34.5\pm3.5$ s was obtained in agreement to the values obtained by Nagourney, Sandberg, and Dehmelt[6] of 32 ± 5 s and Plumelle *et al.*[21] of 47 ± 16 s.

D. Estimate of the quenching rate coefficient of Ar

For Ar, the quenching rate was of such a small magnitude ($<2000\ s^{-1}\ Pa^{-1}$) that large partial pressures of Ar were required ($P>10^{-5}$ Pa) so that the quenching contri-

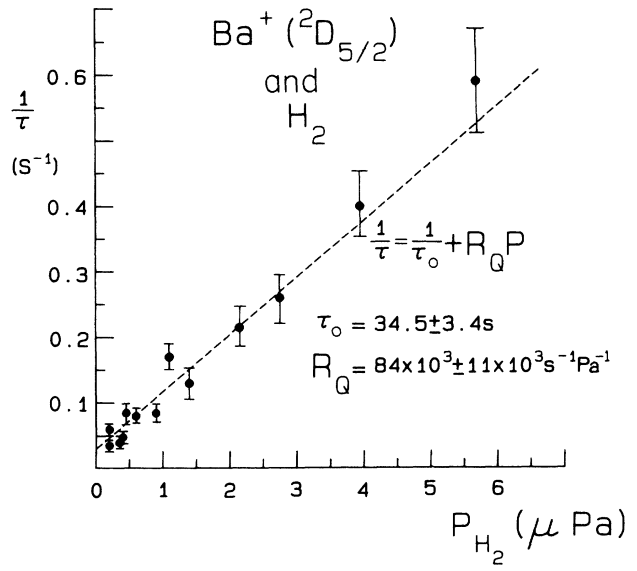

FIG. 6. Plot of observed $5d\ ^2D_{5/2}$ metastable level lifetime as a function of hydrogen background pressure. The dashed line is the fitted value using the final determined quenching rate coefficient for hydrogen.

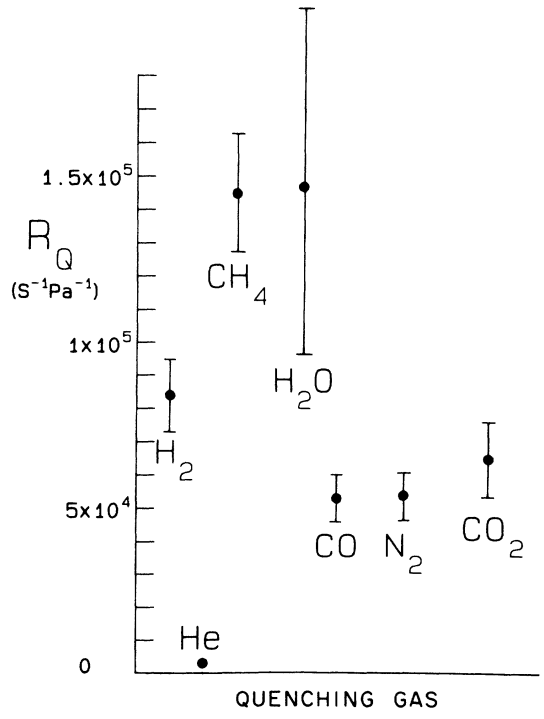

FIG. 7. Summary of $5d\ ^2D_{5/2}$ quenching coefficients for gases used in the present study.

TABLE I. Summary of quenching data for the $5d\,^2D_{5/2}$ level of Ba^+ including quenching coefficients, rate constants, and cross sections for quenching. Also given is the mean velocity $\langle v_r \rangle$ of the quenching gas atom relative to the Ba^+ atom. The numbers in parentheses represent the error.

Gas	Quenching coefficient R_Q ($s^{-1}\,Pa^{-1}$)	Rate constant $\langle \sigma v \rangle$ ($10^{-16}\ m^3\,s^{-1}$)	Mean velocity $\langle v_r \rangle$ ($m\,s^{-1}$)	Cross section $\langle \sigma \rangle$ ($10^{-20}\ m^2$)
H_2	84 000(11 000)	3.5(0.5)	1776(9)	19(3)
He	2400(600)	0.10(0.03)	1256(6)	0.79(0.26)
CH_4	145 000(19 000)	6.0(0.8)	628.0(3.1)	95(13)
H_2O	145 000(48 000)	6.0(2.0)	592.1(3.0)	101(34)
CO	53 000(7000)	2.2(0.3)	474.7(2.4)	46(6)
N_2	55 000(7000)	2.3(0.3)	474.7(2.4)	48(7)
Ar	1600(1300)	0.07(0.05)	397.1(2.0)	1.7(1.3)
CO_2	65 000(12 000)	2.7(0.5)	378.7(1.9)	71(13)

bution of this gas was comparable to other residual gases. Unfortunately, when employing such high pressures, it was found that the mass spectrometer sensitivity to Ar became nonlinear with respect to the ion gauge[19] and that the mass spectrometer sensitivity to the residual gases were perturbed due to the presence of the large background of Ar. In order to obtain an estimate of the quenching rate coefficients for Ar, the $5d\,^2D_{5/2}$ lifetime was measured for various proportions of residual background gas while keeping the total Ar pressure approximately constant. In these studies, the quenching due to H_2 dominated (forming an estimated 60% of the quenching events) with residual CO contributing approximately 23% to the quenching. The effects of other residual gases are small compared to the remaining quenching caused by the Ar, atoms which made up about 12% of the total quenching. If we assume that the presence of Ar has changed the mass spectrometer sensitivity by α such that $P_{T,i}=\alpha P_{m,i}$, where P_T is the true pressure of gas species i, and P_m is the measured pressure, and α is constant for fixed Ar pressure, the observed quenching rate is given by

$$R_{\rm obs}=(1/t_0)+R_{Q,\rm Ar}P_{\rm Ar}+\sum_i R_{Q,i}\alpha_i P_{m,i}\ , \qquad (7)$$

where the summation over the residual gas species i are dominated by H_2 and CO. Assuming the increasing sensitivity α does not vary much between H_2 and CO, we may thus plot $(R_{\rm obs}-1/t_0)/P_{\rm Ar}$ versus $\sum_i (R_{Q,i}P_{m,i})/P_{\rm Ar}$ and extrapolate to $\sum_i(R_{Q,i}P_{m,i})/P_{\rm Ar}$ being zero, obtaining an estimate of $R_{Q,\rm Ar}$. The obtained R_Q values for the other gas species from Table I were employed together with our previously determined value for the radiative decay rate $(1/t_0)$ and a linear regression fit was performed to obtain the quenching rate coefficient for Ar. Our estimate for the quenching rate is $R_{Q,\rm Ar}=1600\pm(80\%)\ s^{-1}\,Pa^{-1}$.

E. Observation of anomalous dark periods in the quantum jump statistics for H_2O and CO_2

In the presence of CO_2 and H_2O, the quantum-jump dark periods were observed to possess an additional distribution of anomalously long dark periods which were greater than several times the natural radiative lifetime of the $^2D_{5/2}$ level. An analysis of these anomalous events together with their separation from the quenching and radiative decay events are described in detail in a previous work.[20] A number of possible mechanisms were considered for this phenomenon and it has been concluded that for these systems, a metastable bound complex of a quenching gas atom and Ba^+ is being formed. For CO_2, durations of up to 11 min were observed and although the rate of such anomalous dark periods were low (2000 $s^{-1}\,Pa^{-1}$), it was possible to collect a sufficient number of events for a study of the distribution of dark times. The distribution of all quantum jumps >10 times the duration of the quenched $^2D_{5/2}$ lifetime at a CO_2 pressure of $P=3\times10^{-6}$ Pa is shown in Fig. 8. As can be seen, the distribution appears exponential. χ^2 tests of the data show a probability of 0.91 that the data is following an exponential distribution.[20] Hence Ba^+ is being shelved into a long-lived metastable complex with CO_2, which is later destroyed by subsequent collisions allowing return to fluorescence. It turned out that removal of these quantum-jump durations from the data sets for quench-

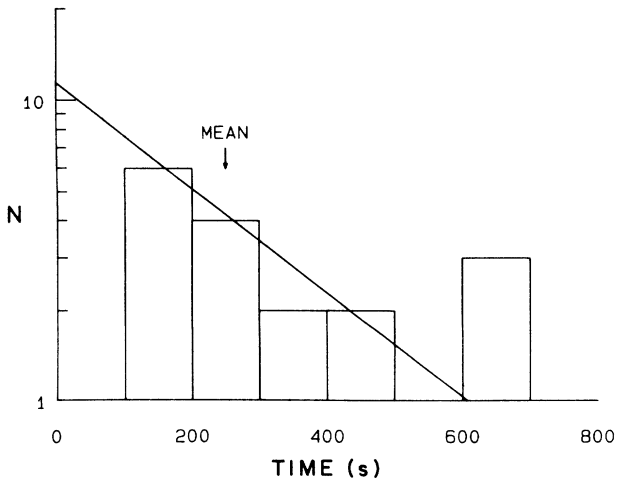

FIG. 8. Distribution of anomalous dark periods observed in the presence of CO_2 ($P=3\times10^{-6}$ Pa) showing long period exponential character.

TABLE II. Review of previous $5d\,^2D$ quenching measurements together with the region of quenching gas pressure employed during the study.

Reference	Gas	Rate coefficient $\langle\sigma v\rangle$ (10^{-16} m^{3}s^{-1})	Level	Pressure regime (Pa)
22	He	0.12	$5d\,^2D_{3/2}$	10^{-4}
23	H_2	0.08–0.8	$5d\,^2D_{3/2}$	10^{-1}
6	unknown	8	$5d\,^2D_{5/2}$	10^{-8}
24	He	0.0030(0.0002)	$5d\,^2D_{3/2}$, $^2D_{5/2}$	10^{-4}–10^{-1}
24	Ne	0.0051(0.0004)	$5d\,^2D_{3/2}$, $^2D_{5/2}$	10^{-4}–10^{-1}
24	H_2	0.37(0.03)	$5d\,^2D_{3/2}$, $^2D_{5/2}$	10^{-4}–10^{-1}
24	N_2	0.44(0.03)	$5d\,^2D_{3/2}$, $^2D_{5/2}$	10^{-4}–10^{-1}

ing was straightforward since the mean anomalous dark period was much longer than the mean lifetime of the quenched $^2D_{5/2}$ level and the two distributions can be well separated (see Sec. II C).

Experiments with H_2O also showed anomalous dark states for the ion; however, due to presumably more permanent binding, the ion does not return from the dark state (however, its presence within the trap was confirmed[20]). As with the results for CO_2, the rate of formation of the dark state was an increasing function of partial pressure. An order of magnitude estimate has been determined using our observations and is determined to be 6000 s^{-1} Pa^{-1}.

IV. DISCUSSION

A. Comparison of present experimental quenching results with those previously obtained

A summary of previous measurements of the quenching rate coefficient as a function of pressure (R_Q) for background gas at $T=300$ K and the quenching rate constant ($\langle\sigma v\rangle$) of the Ba^+ metastable $5d\,^2D$ levels are given in Table II. The quenching rate constants for the $^2D_{3/2}$ level should be quite similar to that of the $^2D_{5/2}$ state. With the exception of the results by Nagourney, Sandberg, and Dehmelt,[6] previous work employed the use of large trapped ion clouds of 10^5–10^6 ions within the trap with quenching gas pressures in the range of 10^{-1}–10^{-4} Pa. In Ref. 6, the experiment employed a single trapped Ba^+ atom in a pressure regime of 10^{-8} Pa, where it was found that the $^2D_{5/2}$ lifetime of $t=30\pm3$ s at $P=1.1\times10^{-8}$ Pa decreased by 25% when the background pressure as increased to 6.0×10^{-8} Pa.[6] The background gas composition, in this experiment was not analyzed, but in analogy to most ultra-high-vacuum systems, would be primarily composed of hydrogen.

When a comparison of the previous results is made with the present study, it would appear that the trapped-ion-cloud experiments performed at a factor of 10^4 higher pressures indicate a lower quenching rate constant. The results by Schneider and Werth[22] for He agree very well with the present result, while the results by Hermanni and Werth[24] seem to indicate a much lower rate constant by a factor of 33 for He, 9.5 for H_2, and 5 for N_2. The results by Nagourney, Sandberg, and Dehmelt would be quite consistent with the present results, since the sensitivity of ion gauges to gases such as hydrogen [0.3 for H_2 (Ref. 19)] is lower than the standard calibration relative to nitrogen.

B. Comparison of present quenching results with classical ion-molecule collision theory

A quantitative comparison of the obtained quenching results from the single, trapped Ba^+ system was made with current classical ion-molecule collision theory[25] for all quenching gas species used. For all species, the collision rate constant due to pure induced polarization of the quenching gas by the stationary Ba^+ atom (Langevin

TABLE III. Comparison of calculated classical ion-molecule collision rate constants with the observed $5d\,^2D_{5/2}$ quenching rate constants for various quenching gases used.

Gas	Polarizability ability α (10^{-24} cm^3)	Dipole moment μ_D (D)	Collisional rate constant $\langle\sigma v\rangle_{coll}$ (10^{-16} m^{3}s^{-1})	Quenching rate constant $\langle\sigma v\rangle_{quench}$ (10^{-16} m^{3}s^{-1})	Ratio
H_2	0.80		15	3.5(0.5)	0.23
He	0.20		5.3	0.10(0.03)	0.02
CH_4	2.6		10.	6.0(0.8)	0.60
H_2O	1.5	1.9	20.	6.0(0.8)	0.30
CO	2.0	0.11	7.0	2.2(0.3)	0.31
N_2	1.7		6.6	2.3(0.3)	0.35
Ar	1.6		5.3	0.07(0.05)	0.01
CO_2	2.9		7.0	2.7(0.5)	0.38

reaction rate coefficient) was calculated using available values for the molecular polarizability,[26,27] which are given in Table III. For such pure polarization cases, the rate coefficient is given by

$$k=\langle \sigma v \rangle = 2\pi q(\alpha/\mu)^{1/2} , \quad (8)$$

where q is the charge of the ion in esu, α is the polarizability in cm^3, and μ is the reduced mass of the Ba^+-quenching gas molecule system in g. In the case of H_2O, and CO, the presence of a permanent dipole moment for the molecule necessitated the inclusion of ion-dipole attraction. In this case, the average dipole orientation theory[25,28,29] (ADO) was applied for the calculation of an additional increase in the rate coefficient. Calculation of the slight increase in the rate coefficient for CO_2 due to the presence of a permanent quadrupole moment was also performed.[25,30] Corrections in the above rate coefficients were made to account for the fact that the massive Ba^+ atom ($m=138$ amu) has been laser cooled to a much lower temperature (<10 K) than the lighter background gas (298 ± 3 K), which resulted in small corrections to the rate coefficient ($<5\%$).

When a comparison is made between the present experimental results for the quenching of the $5d\ ^2D_{5/2}$ level and the classical ion-molecule collision rates, it is apparent that for the molecular quenching gases, the values are quite comparable. In the case of H_2O, CO, N_2, and CO_2, the ratio of the classical collision rate to the determined quenching rate yields a similar ratio of 0.3 within 15%. For these molecules, a quenching event thus occurs on average after three classical ion-molecule collisions. For H_2 being considerably lighter than the other molecules the ratio is slightly smaller, while CH_4 appears to possess extremely efficient quenching (ratio $=0.60$), indicating that on the average most classical ion-molecule collisions, a quenching of the $^2D_{5/2}$ level will occur. The greater efficiency of quenching by CH_4 is presumably due to the many degrees of freedom in the pentatomic molecule which aid in the quenching of the Ba^+ metastable atomic state. In contrast, it can clearly be seen that atomic gases such as He and Ar display a much smaller observed quenching rate to classical collision rate by almost two orders of magnitude. Since the first excited electronic state transitions for He and Ar like at xuv and vuv transition energies, it is clear that internal energy transfer between collision partners does not take place and subsequent quenching efficiency is substantially reduced.

V. CONCLUSIONS

In summary, a single barium ion was held in a radio-frequency trap and excited by continuous wave laser light which provided laser cooling and strong fluorescence emission from the ion. By indirect excitation into the $5d\ ^2D_{5/2}$ level, quantum jumps in the fluorescence were observed. By exposing the ion to well-characterized background gas environments at low pressure (10^{-8}–10^{-5} Pa), collisional quenching of the metastable level resulting in shortening of the mean dark periods were studied. An analysis of the quantum-jump durations for gas pressure variations with H_2, He, CH_4, H_2O CO, N_2, Ar, and CO_2 yielded accurate quenching rate constants of these gases for the $5d\ ^2D_{5/2}$ level of Ba^+. The present results provide the first quantitative measurement of individual gas collisional quenching rates for a single-atom system. In addition, by extrapolating the observed quantum-jump results to zero pressure, an improved value of $t_0=34.5\pm3.5$ s was obtained for the natural lifetime of the $5d\ ^2D_{5/2}$ level in agreement with previous results.

Theoretical calculations of the classical ion-molecule collisional rate constants were performed using current theory including pure polarization and ion-dipole effects. A comparison of the experimental quenching rate and calculated classical collision rate constants show that for the molecular gases studied, the quenching rate constants are comparable to the collision rate with a ratio of quenching to collision rate being 0.3 for most molecular gases, while CH_4 yielded a ratio of 0.6. For the atomic gases of He and Ar, the quenching rate constants were found to be two orders of magnitude below the theoretical collision rates showing the inefficiency of these systems in quenching.

ACKNOWLEDGMENTS

We would like to thank W. Berger for suggestions and expert technical assistance in the construction and operation of the experiment. The insightful suggestions and discussions provided by G. R. Hanes are greatly appreciated. We would like to thank A. H. Bass for expert assistance in the calibration of the pressure measurements.

APPENDIX: CALCULATION OF RAMAN SCATTERING RATE OUT OF THE $5d\ ^2D_{5/2}$ LEVEL BY THE DRIVING LASER FIELDS

It has been shown by Sauter and co-workers[7,12] that the presence of the $6p\ ^2P_{1/2}$–$6s\ ^2S_{1/2}$ (493 nm) and $6p\ ^2P_{1/2}$–$5d\ ^2D_{3/2}$ (650 nm) excitation and laser cooling fields may induce Raman transitions into and out of the $5d\ ^2D_{5/2}$ state if these fields are sufficiently intense. In this section, the Raman induced transition rate for a single Ba^+ atom in the $5d\ ^2D_{5/2}$ level subject to excitation on the S-P and P-D transitions is estimated.

For the Ba^+ system, the 493- and 650-nm photon energies are near only the first five energy levels of the atom. Other levels are sufficiently distant that contributions via Raman scattering are negligible. Hence the levels involved are those depicted in Fig. 2. For Raman scattering, enhancement via coupling from the initial state to a nearby intermediate level must be electric dipole allowed. In our case, the sole nearby intermediate level, which couples from the $5d\ ^2D_{5/2}$ state, is the $6p\ ^2P_{3/2}$ level. Via this intermediate level, scattering to the $6s\ ^2S_{1/2}$ ground state or the $5d\ ^2D_{3/2}$ level can occur. It has been shown[31] that the cross section for Raman scattering for a single atom, including the finite linewidth of the state, is

$$\sigma=\sum_{f,\omega}\frac{6\pi c^2}{\omega_i^2}\frac{\gamma_{i1}\gamma_{if}}{(\omega_i-\omega)^2+\gamma_i^2} , \quad (A1)$$

where scattering takes place from initial state $|1\rangle$ via intermediate state $|i\rangle$ to final state $|f\rangle$. $\gamma_{i,j}$ is the decay width from state i to j and γ_i is the total decay width out of state i. The transition frequency from state $|1\rangle$ to state $|i\rangle$ is ω_i, while ω is the actual driving field frequency. By relating the decay width in terms of the spontaneous-emission rates out of the levels $A_{i,j}$, and converting our cross section into a rate for induced transition out of the metastable level, we have

$$R_{\text{tot}}=\sum_{f,\omega}\frac{6\pi c^2}{\hbar\omega\omega_i^2}\frac{A_{i,1}A_{i,f}I_\omega}{4(\omega_i-\omega)^2+A_i^2}\ , \tag{A2}$$

where the intensity of the driving field at frequency ω is I_ω. From the spontaneous-emission rate for the $6p\ ^2P_{3/2}$ level provided by Gallagher[32] and the transition frequencies for the energy levels, we have calculated the total Raman transition rate out of the $5d\ ^2D_{5/2}$ to be

$$R_{\text{tot}}=(2.6\times10^{-8})I_{P\text{-}D}+(1.3\times10^{-9})I_{S\text{-}P}\ , \tag{A3}$$

where $I_{P\text{-}D}$ and $I_{S\text{-}P}$ are the light field intensities in W m^{-2} of the ion for the P-D and S-P transitions, respectively. Using our beam diameter of $D=250$ μm and the maximum incident laser powers used of $P=100$ μW, the total transition rate due to Raman scattering out of the $5d\ ^2D_{5/2}$ level is $R=6\times10^{-5}\ \text{s}^{-1}$, which is small compared to the natural radiative decay of the $5d\ ^2D_{5/2}$ level of $1/t_0=0.03\ \text{s}^{-1}$.

[1]H. G. Dehmelt, Phys. Rev. Scr. **T22**, 120 (1988).

[2]W. M. Itano, J. C. Bergquist, and D. J. Wineland, Science **237**, 612 (1987).

[3]J. C. Bergquist, W. M. Itano, and D. J. Wineland, Phys. Rev. A **36**, 428 (1987).

[4]H. Dehmelt, IEEE Trans. Instrum. Meas. **IM-31**, 83 (1982).

[5]H. Dehmelt, N. Yu, and W. Nagourney, Proc. Natl. Acad. Sci. U.S.A. **86**, 3938 (1989).

[6]W. Nagourney, J. Sandberg, and H. G. Dehmelt, Phys. Rev. Lett. **56**, 2797 (1986).

[7]Th. Sauter, R. Blatt, W. Neuhauser, and P. E. Toschek, Phys. Rev. Lett. **57**, 1696 (1986).

[8]J. C. Bergquist, R. G. Hulet, W. M. Itano, and D. J. Wineland, Phys. Rev. Lett. **57**, 1699 (1986).

[9]R. J. Cook and H. J. Kimble, Phys. Rev. Lett. **54**, 1023 (1985).

[10]G. Nienhuis, Phys. Rev. A **35**, 4639 (1987).

[11]R. Blatt and P. Zoller, Eur. J. Phys. **9**, 250 (1988), and references therein.

[12]Th. Sauter, R. Blatt, W. Neuhauser, and P. E. Toschek, Opt. Commun. **60**, 287 (1986).

[13]W. Neuhauser, M. Hohenstatt, P. E. Toschek, and H. G. Dehmelt, Appl. Phys. **17**, 123 (1978).

[14]G. Janik, W. Nagourney, and H. G. Dehmelt, J. Opt. Soc. B **2**, 1251 (1985).

[15]D. J. Wineland, W. M. Itano and R. S. VanDyck, Jr. in *Advances in Atomic and Molecular Physics,* edited by David Bates and Benjamin Bederson (Academic, New York, 1983), Vol. 19, p. 135.

[16]J. D. Sankey and A. A. Madej, Appl. Phys. B **49**, 69 (1989).

[17]W. M. Itano and D. J. Wineland, Phs. Rev. A **25**, 35 (1982).

[18]A. A. Madej and J. D. Sankey, in *Atomic Physics II,* Proceedings of the Eleventh International Conference on Atomic Physics, edited by S. Haroche, J. C. Gay, and G. Grynberg (World Scientific, Singapore, 1989), p. 639.

[19]J. D. Sankey and A. H. Bass, Vacuum TAIP (to be published).

[20]J. D. Sankey and A. A. Madej, Appl. Phys. B (to be published).

[21]F. Plumelle, M. Desaintfuscien, J. L. Duchene, and C. Audoin, Opt. Commun. **34**, 71 (1980).

[22]R. Schneider and G. Werth, Z. Phys. A **293**, 103 (1979).

[23]W. Ruster, J. Bonn, P. Peuser, and N. Trautmann, Appl. Phys. B **30**, 83 (1983).

[24]A. Hermanni and G. Werth, Z. Phys. D **11**, 301 (1989).

[25]T. Su and M. T. Bowers, in *Gas Phase Ion Chemistry,* edited by M. T. Bowers (Academic, New York, 1979), Vol. 1, p. 83.

[26]T. M. Miller, in *Chemical Rubber Company Handbook of Chemistry and Physics,* 69th ed, edited by R. C. Weast (C.R.C., Boca Raton, 1988), p. E-68.

[27]J. Vanier and C. Audoin, in *The Quantum Physics of Atomic Frequency Standards* (Hilger, Bristol, 1989), p. 328.

[28]T. Su and M. T. Bowers, Int. J. Mass Spectrom. Ion Phys. **12**, 347 (1973).

[29]T. Su, E. C. F. Su, and M. T. Bowers, J. Chem. Phys. **69**, 2243 (1978).

[30]T. Su and M. T. Bowers, Int. J. Mass Spectrom. Ion Phys. **17**, 309 (1975).

[31]R. Loudon, in *The Quantum Theory of Light* (Oxford University Press, Oxford, 1983), p. 322. Note that the formula given by Loudon is smaller by a factor of 3 since he has orientation averaged for large numbers of atoms.

[32]A. Gallagher, Phys. Rev. **157**, 24 (1967).